materials

MDPI

Article

Physical and Dielectric Properties of Ni-Doped In_2S_3 Powders for Optical Windows in Thin Film Solar Cells

Abdelmajid Timoumi [1,*], Walid Belhadj [1], Salah Noaiman Alamri [2] and Mohamed Khalil Al-Turkestani [1]

[1] Physics Department, Faculty of Applied Science, Umm AL-Qura University, Makkah P.O. Box 715, Saudi Arabia; wbbelhadj@uqu.edu.sa (W.B.); mkturkestani@uqu.edu.sa (M.K.A.-T.)
[2] Physics Department, Faculty of Science, Taibah University, Madinah P.O. Box 30002, Saudi Arabia; alamrisaleh@yahoo.com
* Correspondence: aotemoume@uqu.edu.sa; Tel.: +966-56-270-39-45

Abstract: This paper reports the effect of Nickel (Ni) on indium sulfide (In_2S_3) powder. This work presents a systematic study of the physical and dielectric properties of $In_{2-x}S_3Ni_x$ powders with 0, 2, 4, and 6 at.% of nickel. Doped and undoped samples were investigated by X-ray powder diffraction (XRD), energy dispersive X-ray spectroscopy, thermal gravimetric analysis, Fourier transform infrared (FTIR) spectroscopy, Raman spectroscopy, scanning electron microscopy (SEM), and impedance spectroscopy. XRD patterns revealed that each $In_{2-x}S_3Ni_x$ composition was crystalline, which was also confirmed by the FTIR results. The presence of Ni in the samples was confirmed by energy dispersive spectroscopy (EDS). The Raman studies show different peaks related to the In_2S_3 phase and do not reveal any secondary phases of In–Ni and Ni–S. The SEM images of the undoped and Ni-doped In_2S_3 samples indicated a correlation between dopant content and the surface roughness and porosity of the samples. The impedance analysis indicated semiconductor behavior present in all samples, as well as a decrease in resistance with increasing Ni content. This work opens up the possibility of tailoring the properties and integrating Ni-doped In_2S_3 nanocomposites as thin film layers in future solar cells.

Keywords: dielectric properties; doping; impedance spectroscopy; In_2S_3; nickel; solar cells

check for updates

Citation: Timoumi, A.; Belhadj, W.; Alamri, S.N.; Al-Turkestani, M.K. Physical and Dielectric Properties of Ni-Doped In_2S_3 Powders for Optical Windows in Thin Film Solar Cells. *Materials* **2021**, *14*, 5779. https://doi.org/10.3390/ma14195779

Academic Editor: Jana Bidulská

Received: 19 August 2021
Accepted: 26 September 2021
Published: 3 October 2021

Publisher's Note: MDPI stays neutral with regard to jurisdictional claims in published maps and institutional affiliations.

Copyright: © 2021 by the authors. Licensee MDPI, Basel, Switzerland. This article is an open access article distributed under the terms and conditions of the Creative Commons Attribution (CC BY) license (https://creativecommons.org/licenses/by/4.0/).

1. Introduction

The inorganic compound indium sulfide (In_2S_3) recently gained considerable attention as an optical window material in solar photovoltaic cells. In_2S_3 is as well non-toxic and more environmentally friendly compared to other optical window materials such as cadmium sulfide (CdS). In addition, In_2S_3 is an n-type semiconductor that crystallizes at atmospheric pressure in three polymorphic forms (named α, β, and γ) as a function of temperature [1]. These remarkable characteristics of In_2S_3 combined with its eco-friendly nature [2,3] make it well-suited for use in a variety of applications that are fabricated by different processing methods [4–7]. In_2S_3 is generally used in photovoltaic applications [8], semiconductor batteries [9], and photoelectrochemical cells [10,11]. Our previous research [12–20] included detailed investigations of several materials, including thin film indium sulfide. The latter is synthesized in our laboratory and then deposited in the form of thin layers by various techniques such as vacuum thermal evaporation and pyrolysis spray. Various theoretical and experimental studies are made depending on the effect of annealing, temperature, and doping.

In fact, some of the synthesis methods used in our research are relatively complex to manipulate, and a few are costly and time-consuming. Besides our own studies, many other researchers are interested in investigating In_2S_3 powders [21,22]. Hamici M. et al. [21] studied the oxidation process of the crystalline powder of In_2S_3 and thin films obtained by the Dr. Blade Method. They obtained samples showing a band gap varying continuously between 1.94 eV and 3.72 eV and films of intermediate composition. Gorai S. et al. [22]

synthesized the In_2S_3 powder and studied its optical characterization and estimated a band gap value around ~2.12 eV. Other studies [23] are also carried out on CdS powder, it having physical properties close to that of In_2S_3 and which can be used as a thin film for solar cells.

Recently, 3D transition metal impurities in semiconductor nanoparticles attracted significant interest because of their effect on tuning the emission bands [24,25]. A study of commercially doped In_2S_3 will provide an alternative approach for understanding the energy-related applications of this material. In addition, commercial In_2S_3 powder is inexpensive and provides similar encouraging results as laboratory synthesized powders.

In this research, we investigated the effects of doping not only on the structural, morphological, and thermal properties, but also on the dielectric properties of Ni-doped and undoped In_2S_3 powders. The obtained results are presented and discussed below. To our knowledge, this is the first work on In_2S_3 powder doped with nickel.

2. Materials and Methods

2.1. Materials

In_2S_3, a red powder with 99.99% purity, was supplied by the Sigma-Aldrich company and used without purification. Nickel powder (Pulver, Atom Gew. 58.71) in concentrations of 2, 4, and 6 at.% was used to dope In_2S_3. The choice of these concentrations is estimated from our previous work, and, generally, there is a limit to the amount of dopant that could be applied. Each sample consisted of 0.2 g of In_2S_3. To characterize the electrical properties, the total quantity of each sample was pressed into a pellet 13 mm in diameter and 1 mm thick. Two silver paste electrodes were placed on both sides of the pellet and were connected to copper wires.

2.2. Experimental Methods

To characterize the structural properties of the $In_{2-x}S_3Ni_x$ powder, we used X-Ray diffraction (XRD; Cu-Kα = 1.5418 Å, Shimadzu XRD-6000, Shimadzu, Kyoto, Japan). A thermogravimetric analysis (TGA) was performed on the undoped sample employing a TGA-1000 analyzer (Navas Instruments, Conway, SC, USA). Scanning Electron microscopy (SEM; Supers can SSX-550, Shimadzu, Japan) was used to analyze the surface morphology of the samples. To investigate the crystal phases, we used Raman spectroscopy (RS; 532 nm laser, Senterra, Bruker, Billerica, MA, USA). The complex impedance parameters were investigated as a function of frequency (10 Hz–13 MHz) using a computer-controlled impedance analyzer (Agilent 4294A, Agilent, Santa Clara, CA, USA). The entire experimental system is shown in Figure 1.

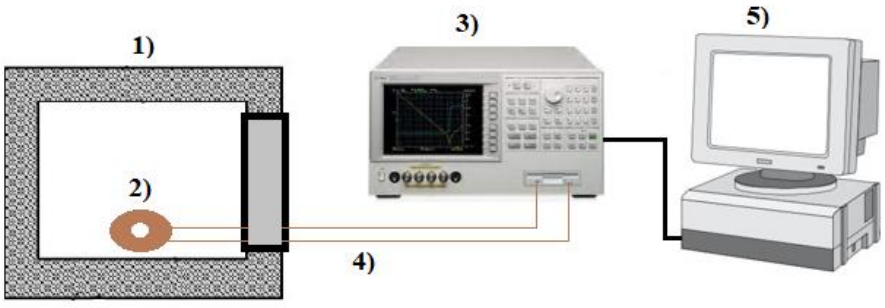


Figure 1. Schematic diagram of experimental system: (**1**) furnace, (**2**) pellet with electrodes, (**3**) impedance analyzer, (**4**) copper wires, and (**5**) computer.

3. Results and Discussion

3.1. XRD and EDS Analysis

X-ray diffraction (Cu–Kα = 1.5418 Å) was used to analyze the structures of the In_2S_3 and $In_{2-x}S_3Ni_x$ samples. Figure 2 shows that all samples were crystalline. This result agrees with that obtained by Lucena et al. [26]. The appearance of other peaks is also apparent

depending on the increase in the dopant level at 2θ angles of 44°, 52°, and 77°, as indicated by the green squares in Figure 2. These peaks are most likely the residual stress in the sample caused by the difference in ionic size between Ni^{2+} (0.70 Å) and In^{3+} (0.80 Å) [27]. No other phase corresponding to the nickel impurity was detected, which is explained by the fact that the Ni ions occupy sulfur substitution positions and do not change the crystal system of the material.

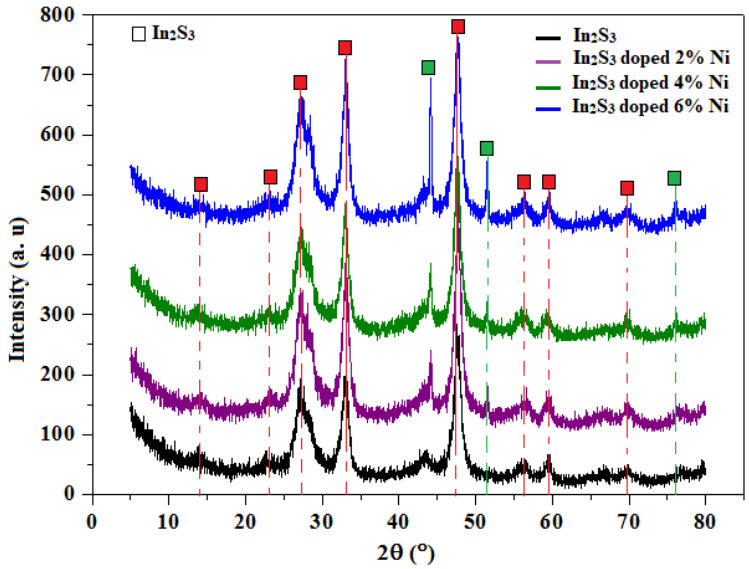


Figure 2. XRD patterns of In_2S_3 and In_2S_3 doped with (2, 4, and 6 at.%) Ni.

A compositional analysis was performed using energy-dispersive X-ray spectroscopy (EDS). The EDS pattern of the undoped In_2S_3 samples (Figure 3) shows the presence of indium and sulfur elements in an atomic percentage ratio of 2/3 for In:S. The other unidentified peaks were attributed to the glass substrate.

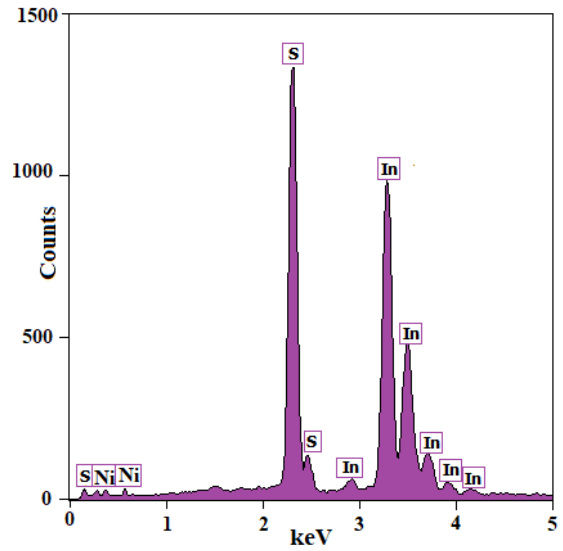


Figure 3. The EDS pattern of the undoped In_2S_3 powder.

The EDS analysis also confirmed the presence of different nickel contents for each sample. The atomic percentages of the elements in the samples are listed in Table 1, which indicates that when the Ni content increased, the quantity of indium decreased slightly,

and the percentage of sulfur remained constant. It is expected that Ni doping of the In_2S_3 samples was substitutional.

Table 1. Chemical composition of In_2S_3 and In_2S_3:Ni samples.

Ni:In Ratio in Powder Samples	Elements		
	In (at.%)	S (at.%)	Ni (at.%)
Undoped	40.54	59.46	0
2%	39.47	58.50	2.04
4%	40.12	57.08	2.80
6%	39.63	56.70	3.67

3.2. Thermal Analysis

The thermal behavior of the In_2S_3 material was studied using a TGA. As shown in Figure 4, the TGA thermograms show that the untreated In_2S_3 material is thermally stable at temperatures beyond 400 °C, and the weight loss is approximately 5%. This behavior is attributed to the purity and crystallinity of the material.

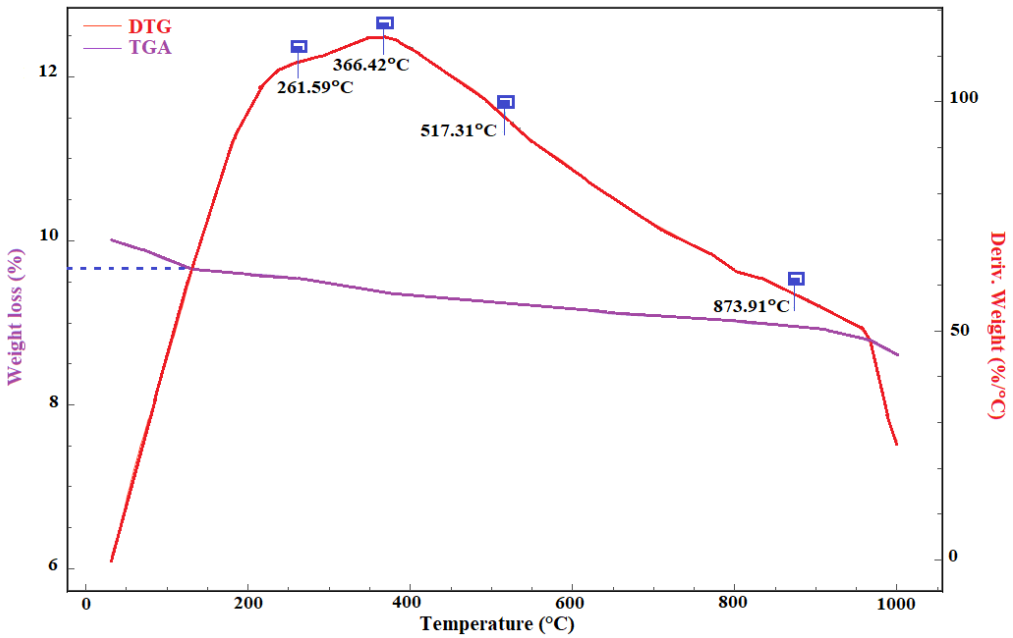


Figure 4. TGA and DTG analysis of the undoped In_2S_3 powder.

3.3. Raman Analysis

Figure 5 presents the experimental Raman spectra for all samples in the range 100–600 cm^{-1}, which indicates the presence of In_2S_3 phase modes, in agreement with the results obtained by Kraini et al. [28]. The active modes were observed at 115, 210, 308, and 365 cm^{-1}, confirming their composition and structure [29]. The indicated modes produced broad peaks with low intensity. At about 220 cm^{-1}, the observed peak corresponds to the presence of elemental sulfur in the structure of the thin film. At near 300 cm^{-1}, the obtained Raman mode is attributed to the Eg mode of the In–S bond. The position of the peak and the half-width of the phase of Raman bands were independent of the Ni-doping content. However, there was a slight change in the relative intensity of the Raman band at 315 cm^{-1}, which appears to correlate with the changes observed by X-ray diffraction for the sample containing 6 at.% Ni. We also noticed the absence of secondary phases, which is in good agreement with the obtained XRD results.

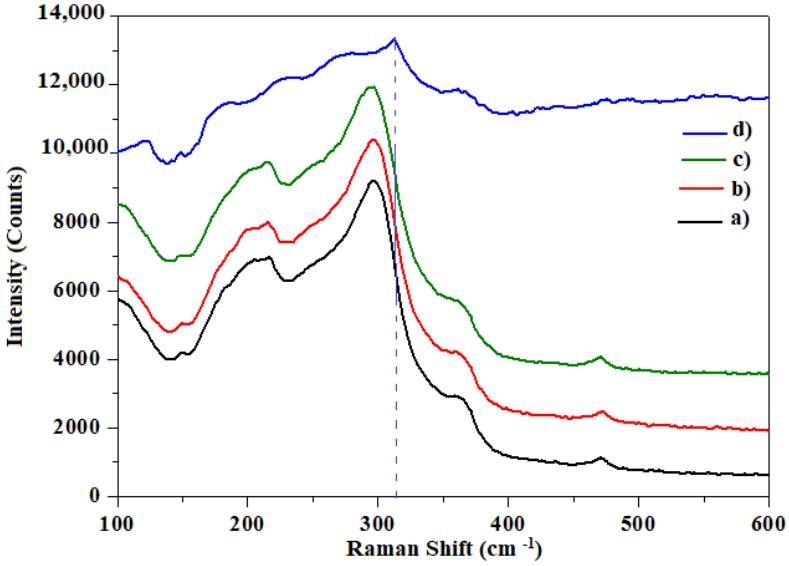


Figure 5. Raman spectra of (**a**) undoped In_2S_3 and In_2S_3 doped with (**b**) 2 at.%, (**c**) 4 at.%, and (**d**) 6 at.% Ni.

3.4. FTIR

FTIR spectral fingerprints for each sample in the wavenumber range of 100 to 600 cm^{-1} provided details of the chemical structure. Figure 6 shows the presence of three absorption bands at 1000–1500 cm^{-1} corresponding to the extension of the C–H and O–H bonds, and also at 900–1200 cm^{-1} and approximately 800 cm^{-1} corresponding to the stretching of the C=O bonds and the O–H band, respectively.

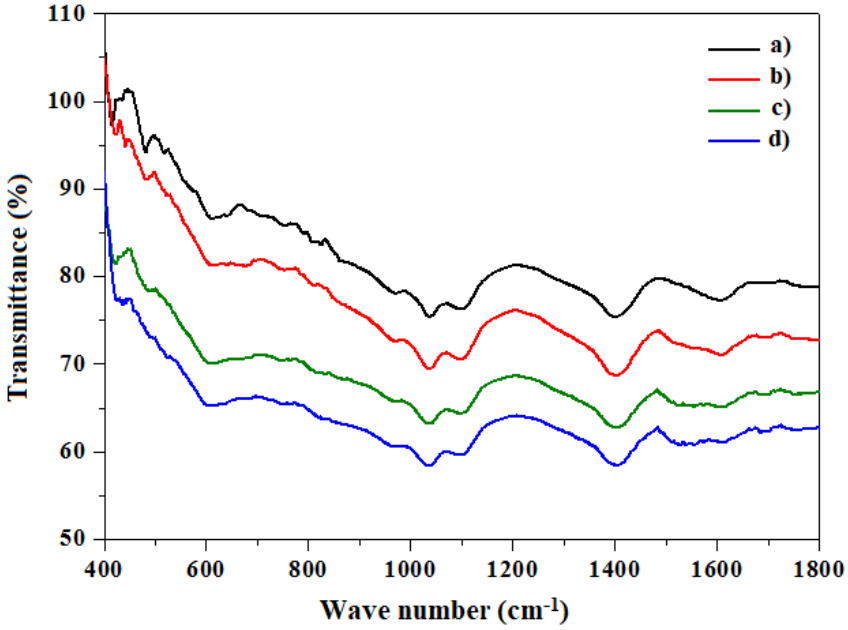


Figure 6. FTIR spectra of (**a**) undoped In_2S_3 and In_2S_3 doped with (**b**) 2, (**c**) 4, and (**d**) 6 at.% Ni.

3.5. SEM

Figure 7 shows the SEM images of the undoped In_2S_3 and Ni-doped In_2S_3 samples. The surfaces show highly irregular surface roughness and porosity that increase with increasing the Ni-doping concentration, as shown in Figure 7d. There was also a clear increase in the number of grains with increasing Ni content, as well as surface homogeneity.

This is probably due to Ni filling the pores on the surface of the composite layer. From the SEM images, the surface roughness obviously increased after doping.

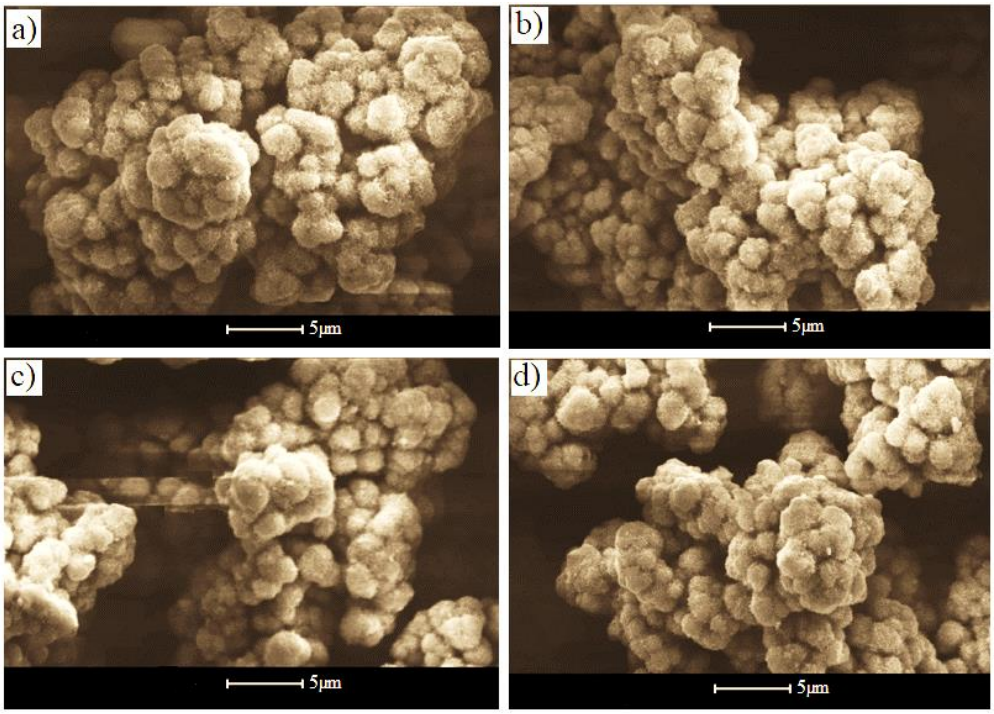


Figure 7. SEM images of (**a**) undoped In_2S_3 and In_2S_3 doped with (**b**) 2, (**c**) 4, and (**d**) 6 at.% Ni.

3.6. Electrical Impedance

Currently, much work is interested in electrical and dielectric properties of materials [30–32]. Nyquist plots are commonly used for characterizing electrical and dielectric properties of semiconductors' materials [33–36], so we constructed Nyquist plots for our In_2S_3 powder samples. Doping is one of the approaches used to minimize electrical resistivity [37]; therefore, to study the dopant effects on the dielectric behavior of the In_2S_3 samples, we used impedance spectroscopy (IS). The undoped and doped In_2S_3 powders were pressed into a pellet (13 mm diameter and 1 mm thickness) prior to applying silver paste, which served as an electrical contact. The Nyquist plots obtained for all samples in the frequency range of 10 Hz to 30 MHz and at different temperatures of 200–400 °C are presented in Figure 8. These Nyquist plots exhibit semi-circular arcs whose centers are located under the real part axis, which suggests a non-Debye-type relaxation phenomenon of the charge carriers [38]. The diameter and shape of the semicircles changed with the temperature, which indicates temperature-dependent semiconductor behavior [39,40]. Initially, the Nyquist diagrams illustrate increases in the semi-circular diameters as the temperature increases above 200 °C [33,41]. However, the semi-circles shifted to lower frequencies, and their diameters decreased after heating to 260–320 °C, indicating a thermally activated electrical conductivity and relaxation time distribution [42]. This phenomenon was observed at 320 °C for pure In_2S_3 and from 280 °C to 260 °C for the Ni-doped samples. Resistance values decreased rapidly with temperature, and the carrier concentration increased with doping because indium sulfide has many vacant indium sites [43].

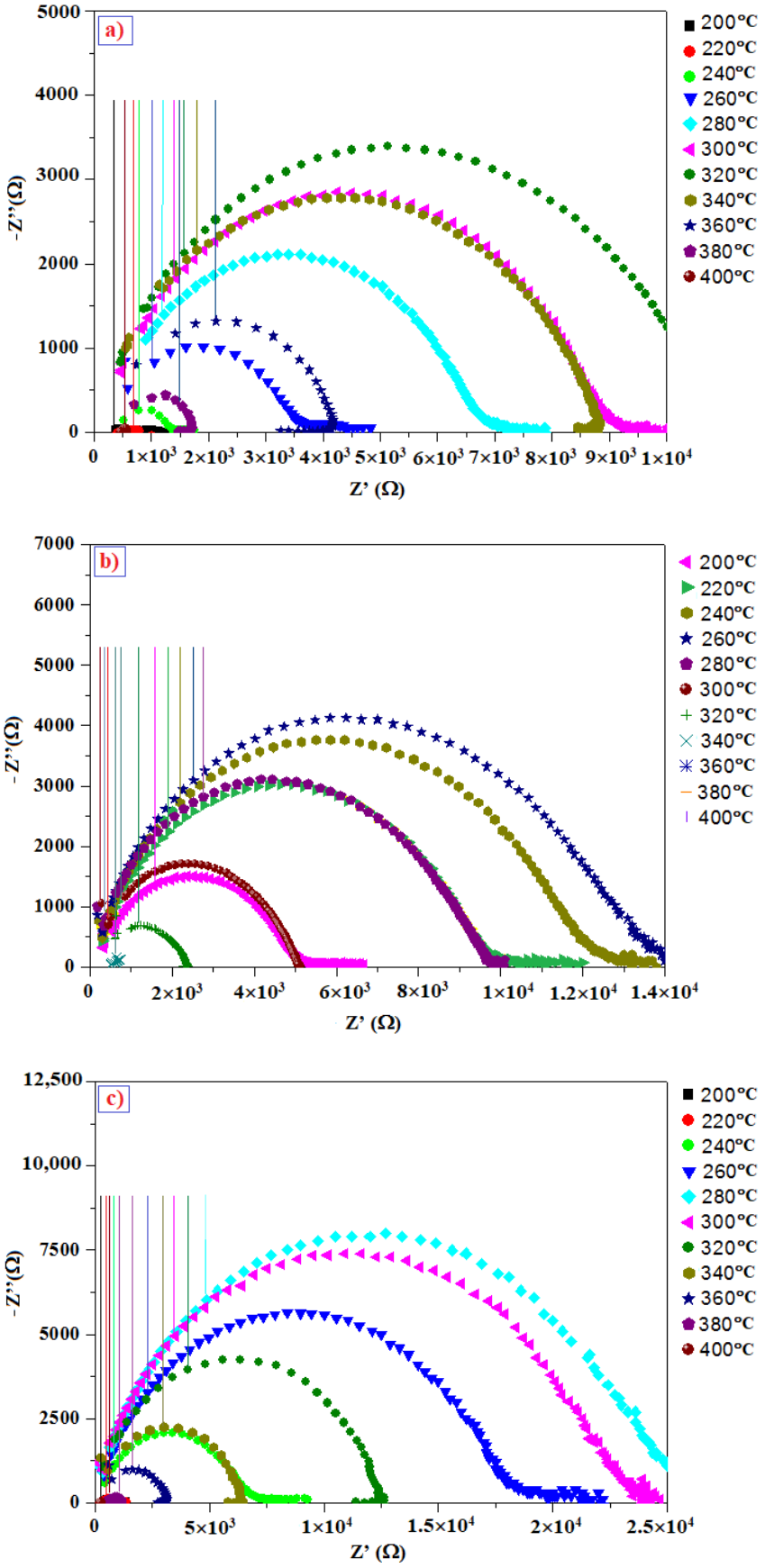


Figure 8. *Cont.*

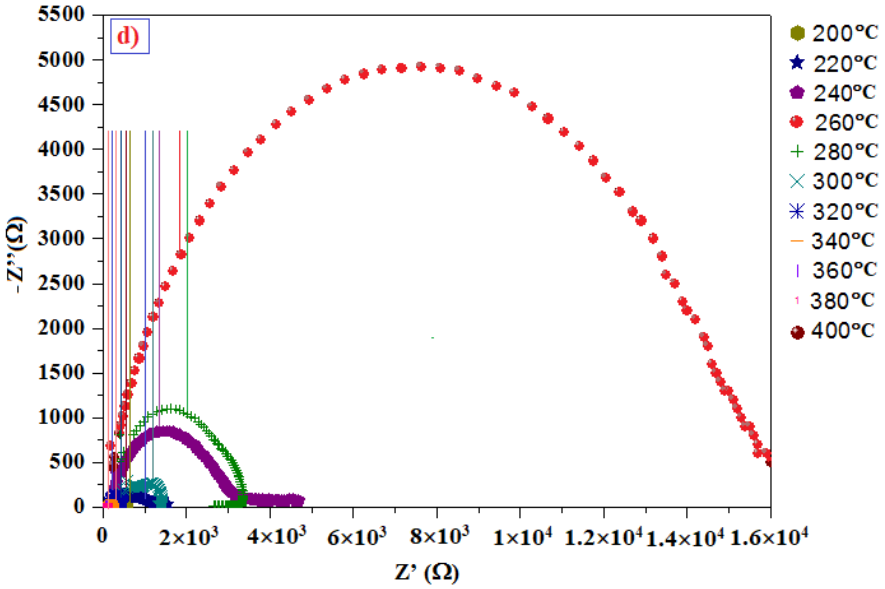


Figure 8. (-Z′′ vs. Z′) plots of (**a**) In_2S_3 and In_2S_3 doped with (**b**) 2, (**c**) 4, and (**d**) 6 at.% Ni and heated to 200–400 °C.

The modeling of the measured impedance spectra and the choice of an appropriate electrical equivalent circuit allow us to consider the electrical phenomena in our undoped and Ni-doped In_2S_3 material. The ZSimpWin 3.10 program was used to compute the circuit parameters. The assigned equivalent circuit for this study is shown in Figure 9, in which the resistance is connected in parallel to the constant phase element impedance (CPE).

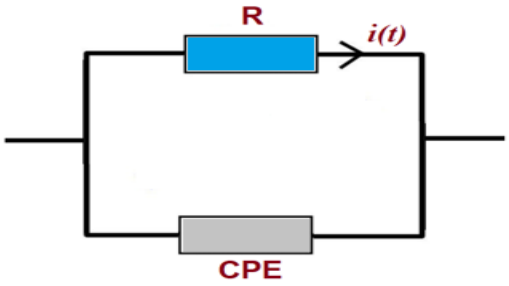


Figure 9. The proposed equivalent circuit.

The CPE impedance (Z_{CPE}) is defined in Equation (1) [44];

$$Z_{CPE} = \frac{1}{Q(j\omega)^{\beta}} \quad (1)$$

where:

Q is a constant value independent of frequency; Ω is the angular frequency; and β is an exponent that measures the arc depression of the CPE impedance [45].

4. Conclusions

In summary, we investigated the effect of doping In_2S_3 powder with nickel on the crystal structure, distribution of dopants, thermal behavior, molecular structure and bonding modes, surface morphology, and electrical impedance. This study showed that Ni doping preserved the crystallinity of each dopant concentration, and no phase changes were observed due to Ni doping. The EDS analysis proved that the In_2S_3 samples had a Ni-rich and S-deficient composition. The SEM images presented in this work showed a

gradual formation of dense samples that were free of cracks with increasing Ni content. The electrical conductance improved with increasing the temperature from a certain characteristic value of the sample. The results obtained in this study highlight the significant effect of doping on the electrical and structural properties of In_2S_3 especially in its powder form. The results reported in this study may facilitate the use of In_2S_3 materials for future applications in photovoltaic devices.

Author Contributions: Conceptualization, A.T., W.B., S.N.A., M.K.A.-T.; Methodology, A.T., W.B., S.N.A., M.K.A.-T.; Data Investigation, A.T., S.N.A.; Supervision, A.T.; Visualization, A.T., W.B., S.N.A., M.K.A.-T.; Writing—Original draft, A.T.; Writing—Review and Editing, contribution by all the authors. All authors have read and agreed to the published version of the manuscript.

Funding: This research was supported by the Scientific Research (19- SCI-1-01-0013) of Umm Al-Qura University, Saudi Arabia.

Institutional Review Board Statement: Not applicable.

Informed Consent Statement: Not applicable.

Data Availability Statement: The data presented in this study are available on request from the corresponding author.

Acknowledgments: The authors would like to thank the Deanship of Scientific Research at Umm Al-Qura University for supporting this work (Grant Code: 19- SCI-1-01-0013).

Conflicts of Interest: The authors declare no conflict of interest. The funders had no role in the design of the study; in the collection, analyses, or interpretation of data; in the writing of the manuscript, or in the decision to publish the results.

References

1. Revathi, N.; Prathap, P.; Miles, R.; Reddy, K.R. Annealing effect on the physical properties of evaporated In2S3 films. *Sol. Energy Mater. Sol. Cells* **2010**, *94*, 1487–1491. [CrossRef]
2. Hsiao, Y.-J.; Lu, C.-H.; Ji, L.-W.; Meen, T.-H.; Chen, Y.-L.; Chi, H.-P. Characterization of photovoltaics with In2S3 nanoflakes/p-Si heterojunction. *Nanoscale Res. Lett.* **2014**, *9*, 32. [CrossRef] [PubMed]
3. Rasool, S.; Saritha, K.; Reddy, K.R.; Bychto, L.; Patryn, A.; Maliński, M.; Tivanov, M.; Gremenok, V. Optical properties of thermally evaporated In 2 S 3 thin films measured using photoacoustic spectroscopy. *Mater. Sci. Semicond. Process.* **2017**, *72*, 4–8. [CrossRef]
4. Sim, Y.; Kim, J.; Chang, S.H.; Choi, C.-J.; Seong, M.-J. Highly luminescent In2S3 thin films with preferred growth direction of [1 0 3]. *Appl. Surf. Sci.* **2021**, *555*, 149706. [CrossRef]
5. De Moure-Flores, F.; Nieto-Z, K.E.; Guillén, C.A.; Gallardo, S.; Quiñones, G.J.G.; Hernández, H.A.; Olvera, L.M.; Zapata, T.M.; Kundriavtsev, Y.; Meléndez, L.M. Effect of the immersion in CdCl2 and annealing on physical properties of CdS:F films grown by CBD. *J. Phys. Chem. Solids* **2013**, *74*, 611. [CrossRef]
6. Hashemi, M.; Heidariramsheh, M.; Ghorashi, S.M.B.; Taghavinia, N.; Mahdavi, S.M. Study on spray-pyrolyzed In2S3 thin films, targeted as electron transport layer in solar energy. *J. Photon-Energy* **2020**, *10*, 024001. [CrossRef]
7. Gao, W.; Liu, W.; Leng, Y.; Wang, X.; Wang, X.; Hu, B.; Yu, D.; Sang, Y.; Liu, H. In2S3 nanomaterial as a broadband spectrum photocatalyst to display significant activity. *Appl. Catal. B Environ.* **2015**, *176–177*, 83–90. [CrossRef]
8. Sarkar, S.K.; Kim, J.Y.; Goldstein, D.N.; Neale, N.R.; Zhu, K.; Elliott, C.M.; Frank, A.J.; George, S.M. In2S3 atomic layer deposition and its application as a sensitizer on TiO_2 nanotube arrays for solar energy conversion. *J. Phys. Chem. C* **2010**, *114*, 17, 8032. [CrossRef]
9. Nehra, S.; Chander, S.; Sharma, A.; Dhaka, M. Effect of thermal annealing on physical properties of vacuum evaporated In2S3 buffer layer for eco-friendly photovoltaic applications. *Mater. Sci. Semicond. Process.* **2015**, *40*, 26–34. [CrossRef]
10. Pulipaka, S.; Koushik, A.K.S.; Deepa, M.; Meduri, P. Enhanced photoelectrochemical activity of Co-doped β-In2S3nanoflakes as photoanodes for water splitting. *RSC Adv.* **2019**, *9*, 1335–1340. [CrossRef]
11. Kwoka, M.; Ottaviano, L.; Szuber, J. AFM study of the surface morphology of L-CVD SnO_2 thin films. *Thin Solid Film.* **2007**, *515*, 8328–8331. [CrossRef]
12. Timoumi, A.; Bouzouita, H.; Kanzari, M.; Rezig, B. Fabrication and characterization of In2S3 thin films deposited by thermal evaporation technique. *Thin Solid Films* **2005**, *480–481*, 124–128. [CrossRef]
13. Timoumi, A.; Bouzouita, H.; Brini, R.; Kanzari, M.; Rezig, B. Optimization of annealing conditions of In2S3 thin films deposited by vacuum thermal evaporation. *Appl. Surf. Sci.* **2006**, *253*, 306–310. [CrossRef]
14. Timoumi, A.; Bouzouita, H.; Rezig, B. Optical constants of Na–In2S3 thin films prepared by vacuum thermal evaporation technique. *Thin Solid Film.* **2011**, *519*, 7615–7619. [CrossRef]

15. Bouguila, N.; Timoumi, A.; Bouzouita, H.; Lacaze, E.; Bouchriha, H.; Rezig, B. Molar ratio S/In effect on properties of sprayed In2S3films. *Eur. Phys. J. Appl. Phys.* **2013**, *63*, 20301. [CrossRef]
16. Bouguila, N.; Timoumi, A.; Bouzouita, H. Vacuum annealing temperature on spray In2S3layers. *Eur. Phys. J. Appl. Phys.* **2014**, *65*, 20304. [CrossRef]
17. Bouguila, N.; Kraini, M.; Timoumi, A.; Halidou, I.; Vazquez-Vazquez, C.; López-Quintela, M.A.; Alaya, S. Substrate temperature effect on properties of sprayed In2S3 films. *J. Mater. Sci. Mater. Electron.* **2015**, *26*, 7639–7648. [CrossRef]
18. Timoumi, A.; Bouguila, N.; Chaari, M.; Kraini, M.; Matoussi, A.; Bouzouita, H. Electrical and dielectric properties of In2S3 synthesized by solid state reaction. *J. Alloys Compd.* **2016**, *679*, 59–64. [CrossRef]
19. Abassi, H.; Bouguila, N.; Timoumi, A. Theoretical Study of the AC Conduction in β-In2S3. *J. Electron. Mater.* **2018**, *47*, 2519–2525. [CrossRef]
20. Timoumi, A.; Belhadj, W.; Alamri, S.; Al Turkestani, M. Experimental studies and new theoretical modeling on the properties of In2S3 thin films. *Opt. Mater.* **2021**, *118*, 111238. [CrossRef]
21. Hamici, M.; Guessoum, K.; Vaillant, L.; Gagou, Y.; Saint-Grégoire, P. Study of the Oxidation Process of Crystalline Powder of In2S3 and Thin Films Obtained by Dr Blade Method. *J. Electron. Mater.* **2019**, *48*, 4715–4725. [CrossRef]
22. Gorai, S.; Guha, P.; Ganguli, D.; Chaudhuri, S. Chemical synthesis of β-In2S3 powder and its optical characterization. *Mater. Chem. Phys.* **2003**, *82*, 974–979. [CrossRef]
23. Alamri, S.N. Structure and optical properties of chunk and powder CdS film prepared by electron beam deposition. *Indian J. Phys.* **2013**, *88*, 259–264. [CrossRef]
24. Masikane, S.C.; McNaughter, P.D.; Lewis, D.J.; Vitorica-Yrezabal, I.; Doyle, B.P.; Carleschi, E.; O'Brien, P.; Revaprasadu, N. Important Phase Control of Indium Sulfide Nanomaterials by Choice of Indium(III) Xanthate Precursor and Thermolysis Temperature. *Eur. J. Inorg. Chem.* **2019**, *2019*, 1421–1432. [CrossRef]
25. Ghosh, S.; Saha, M.; Ashok, V.D.; Chatterjee, A.; De, S.K. Excitation dependent multicolor emission and photoconductivity of Mn, Cu doped In2S3monodisperse quantum dots. *Nanotechnology* **2016**, *27*, 155708. [CrossRef] [PubMed]
26. Lucena, R.; Conesa, J.C.; Aguilera, I.; Palacios, P.; Wahnón, P. V-substituted In2S3: An intermediate band material with photocatalytic activity in the whole visible light range. *J. Mater. Chem. A* **2014**, *2*, 8236–8245. [CrossRef]
27. Timoumi, A.; Zayoud, W.; Sharma, A.; Kraini, M.; Bouguila, N.; Hakamy, A.; Revaprasadu, N.; Alaya, S. Impact of thermal annealing inducing oxidation process on the crystalline powder of In2S3. *J. Mater. Sci. Mater. Electron.* **2020**, *31*, 13636–13645. [CrossRef]
28. Kraini, M.; Bouguila, N.; Moutia, N.; El Ghoul, J.; Khirouni, K.; Vázquez-Vázquez, C. Properties of nickel doped In2S3 thin films deposited by spray pyrolysis technique. *J. Mater. Sci. Mater. Electron.* **2017**, *29*, 1888–1906. [CrossRef]
29. Aldon, L.; Uhrmacher, M.; Branci, C.; Ziegler, L.; Roth, J.; Schaaf, P.; Metzner, H.; Olivier, F.J.; Jumas, J.C. Perturbed angular correlation study of the thiospinel β−In2S3. *Phys. Rev. B.* **1998**, *58*, 11303. [CrossRef]
30. Liu, P.; Ng, V.M.H.; Yao, Z.; Zhou, J.; Lei, Y.; Yang, Z.; Lv, H.; Kong, L.B. Facile Synthesis and Hierarchical Assembly of Flowerlike NiO Structures with Enhanced Dielectric and Microwave Absorption Properties. *ACS Appl. Mater. Interfaces* **2017**, *9*, 16404–16416. [CrossRef] [PubMed]
31. Liu, P.; Yao, Z.; Zhou, J.; Yang, Z.; Kong, L.B. Small magnetic Co-doped NiZn ferrite/graphene nanocomposites and their dual-region microwave absorption performance. *J. Mater. Chem. C* **2016**, *4*, 9738–9749. [CrossRef]
32. Liu, P.; Yao, Z.; Ng, V.M.H.; Zhou, J.; Kong, L.B.; Yue, K. Facile synthesis of ultrasmall Fe3O4 nanoparticles on MXenes for high microwave absorption performance. *Compos. Part A* **2018**, *115*, 371. [CrossRef]
33. Koaib, J.; Bouguila, N.; Abassi, H.; Moutia, N.; Kraini, M.; Timoumi, A.; Vázquez-Vázquez, C.; Khirouni, K.; Alaya, S. Dielectric and electrical properties of annealed ZnS thin films. The appearance of the OLPT conduction mechanism in chalcogenides. *RSC Adv.* **2020**, *10*, 9549–9562. [CrossRef]
34. Chakroun, R.; Jamoussi, B.; Al-Mur, B.; Timoumi, A.; Essalah, K. Impedance Spectroscopy and Dielectric Relaxation of Imidazole-Substituted Palladium(II) Phthalocyanine (ImPdPc) for Organic Solar Cells. *ACS Omega* **2021**, *6*, 10655–10667. [CrossRef]
35. Timoumi, A.A.; Bouguila, N.; Koaib, J.; Al Turkestani, M.K.; Jamoussi, B.; Timoumi, A.; Koiab, J. Study of electrical and dielectric properties of palladium-phthalocyanine (PdPc) in pellet form. *Mater. Res. Express* **2019**, *6*, 055103. [CrossRef]
36. Timoumi, A.; Wederni, M.A.; Bouguila, N.; Jamoussi, B.; AL Turkestani, M.K.; Chakroun, R.; Al-Mur, B. Electrical impedance spectroscopy study of unsubstituted palladium (II) phthalocyanine. *Synth. Met.* **2021**, *272*, 116659. [CrossRef]
37. Tao, H.; Zang, H.; Dong, G.; Zeng, J.; Zhao, X. Raman and infrared spectroscopic study of the defect spinel In21.333S32. *Optoelectron. Adv. Mater.* **2008**, *2*, 356.
38. Aakansha; Deka, B.; Ravi, S.; Pamu, D. Impedance spectroscopy and ac conductivity mechanism in Sm doped Yttrium Iron Garnet. *Ceram. Int.* **2017**, *43*, 10468–10477. [CrossRef]
39. Khosravi, S.H.; Veerapanduyan, V.K.; Vallant, R.; Reichmann, K. Effect of processing conditions on the structural properties and corrosion behavior of TiO_2–SiO2 multilayer coatings derived via the sol-gel method. *Ceram. Int.* **2020**, *46*, 17741. [CrossRef]
40. Ahmad, I.; Akhtar, M.J.; Hasan, M.M. Impedance spectroscopic investigation of electro active regions, conduction mechanism and origin of colossal dielectric constant in Nd1−xSrxFeO3 ($0.1 \leq x \leq 0.5$). *Mater. Res. Bull.* **2014**, *60*, 474. [CrossRef]
41. Tan, F.K.; Hassan, J.; Wahab, Z.A.; Azis, R.S. Electrical conductivity and dielectric behaviour of manganese and vanadium mixed oxide prepared by conventional solid state method. *Eng. Sci. Technol. Int. J.* **2016**, *19*, 2081–2087. [CrossRef]

42. Trabelsi, I.; Jebali, A.; Kanzari, M. Electrical characterization of SnSb4S7 thin films by impedance spectroscopy. *J. Mater. Sci. Mater. Electron.* **2016**, *27*, 4326–4335. [CrossRef]
43. Pistor, P.; Merino, Á.J.M.; León, M.; Michiel, M.; Schorr, S.; Klenk, R.; Lehmann, S. Structure reinvestigation of α-, β- and γ-In2S3. *Acta Crystallogr. B.* **2016**, *72*, 410. [CrossRef] [PubMed]
44. Zoltowski, P. On the electrical capacitance of interfaces exhibiting constant phase element behaviour. *J. Electroanal. Chem.* **1998**, *443*, 149–154. [CrossRef]
45. Jorcin, J.-B.; Orazem, M.; Pébère, N.; Tribollet, B. CPE analysis by local electrochemical impedance spectroscopy. *Electrochim. Acta* **2005**, *51*, 1473–1479. [CrossRef]